Appl. Sci. Converg. Technol. 26(4): 55-61 (2017)
http://dx.doi.org/10.5757/ASCT.2017.26.4.55

Review Paper

Approaches to Reduce the Contact Resistance by the Formation of Covalent Contacts in Graphene Thin Film Transistors

Youngeun Na[a], Jaehyun Han[b,c], and Jong-Souk Yeo[a,b,c]*
[a]*Integrated Science and Engineering Division, Yonsei University*
[b]*School of Integrated Technology, Yonsei University*
[c]*Yonsei Institute of Convergence Technology, Yonsei University*
[a,b,c]*162-1 Songdo-dong, Yeonsu-gu, Incheon 406-840, Republic of Korea*

Received June 22, 2017; revised July 29, 2017; accepted July 30, 2017

Abstract Graphene, with a carrier mobility achieving up to 140,000 cm^2/Vs at room temperature, makes it an ideal material for application in semiconductor devices. However, when the metal comes in contact with the graphene sheet, an energy barrier forms at the metal-graphene interface, resulting in a drastic reduction of the carrier mobility of graphene. In this review, the various methods of forming metal-graphene covalent contacts to lower the contact resistance are discussed. Furthermore, the graphene sheet in the area of metal contact can be cut in certain patterns, also discussed in this review, which provides a more efficient approach to forming covalent contacts, ultimately reducing the contact resistance for the realization of high-performance graphene devices.

Keywords: Graphene, Carrier mobility, Contact resistance, Covalent contacts, Patterning

I. Introduction

Ever since the discovery of the exceptional optical [1-3], electrical [4-6], mechanical [7,8], and thermal [9,10] properties of graphene, it was immediately applied to the areas such as transparent electrodes [11-13], photovoltaic devices [14,15], and electrochemical sensors [16]. Also, the application areas include graphene transistors [17-19] since graphene has a high carrier mobility of up to 140,000 cm^2/Vs at room temperature [20]. Because of the high carrier mobility of graphene, it should ideally have exceptional device performance. However, the two-dimensional material experiences a severe drop in its carrier mobility when realized as the semiconductor channel layer because experimental graphene exhibits several problems that strays it from ideal graphene. Some of those problems are the presence of defects and impurities in the lattice [21], the presence of wrinkles in the sheet [22,23], its interaction with the substrate [24,25], and the presence of photoresist residues [26,27] from imperfect photoresist etching during device fabrication. Because already various effects exist that reduce the mobility, a further decrease should be prevented to take advantage of graphene's exceptional transport properties.

However, the carrier mobility is further reduced during metallization, when the metal electrodes are deposited. The decrease in the mobility is due to the energy barrier that exists at the metal-graphene interface, where the metal comes in contact with the graphene. Hence, contact resistance forms at the interface, which lowers device performance. Contact resistance forms due to the presence of π-bonds in the z-direction in the graphene lattice from the sp^2 hybridization of graphene, the bonds which restrict the metal from strongly binding to the semiconductor sheet during metallization. Hence, when the metal is deposited on graphene using a top-contact mechanism, the metal binds onto the underlying sheet with large coupling length via van der Waals forces because of the presence of the stable π-bonds [28]. The weak adhesion of the metal to the graphene results in the formation of an energy barrier at the interface, which limits carrier transfer and hence lowers the carrier mobility of the device, all effects of contact resistance.

Thus, to realize high-performance graphene devices, contact resistance must be reduced. Throughout the years of graphene research, researchers have discovered various methods to reduce the contact resistance, including work-function engineering [29,30], ultraviolet ozone treatment [31,32], alteration of the device geometry [33,34], and improvement of the surface roughness of graphene [35]. However, these methods are all approaches to strengthen the metal adhesion to the graphene sheet while the device is in a top-contact structure, which is still limited by the weak van der Waals forces at the metal-graphene interface. So, a better approach would be to overcome the energy barrier by eliminating those limiting forces.

*Corresponding author
E-mail: jongsoukyeo@yonsei.ac.kr

That very approach is the formation of metal-graphene covalent contacts at the interface of the device. Covalent contacts are the covalent bonding of the metal to the graphene sheet, and they are made possible by removing a carbon atom from the graphene lattice, exposing dangling σ-bonds to which the metal can bind. Thus, in covalent contacts, because the metal no longer binds to the graphene through van der Waals forces as in top contacts, a shorter bonding distance with large orbital overlap results [20]. By such, the energy barrier at the metal-graphene interface is lowered, and electrons from the metal electrodes can transfer more efficiently to the graphene channel via overlapping orbitals. Consequently, the transmission efficiency (TE) of the carriers is increased, and the contact resistance (R_C) is decreased, as shown in Equation 1:

$$\frac{1}{R_C} = \frac{4q^2}{h}\int_{-\infty}^{\infty} \mathrm{dETE}F_T(E-\mu) \quad (1)$$

where F_T is the thermal broadening function, E is the electron energy, and μ is the chemical potential [36]. The contact resistances are generally measured using a transmission line method (TLM), method, in which the channel lengths of the devices vary to obtain a TLM graph that is composed of the resistance values between each metal-semiconductor contact. The contact resistance value can be extracted from Equation 2 below:

$$R_{total} = \frac{2R_C}{W} + \rho L[\Omega] \quad (2)$$

where R_C is the contact resistance, W is the channel width, L is the channel length, and r is the channel resistivity [28]. Hence, from the graph of the total resistance versus channel length, since the y-intercept of the graph is twice R_C, the contact resistance in the unit can be calculated easily. To obtain the units of $\Omega\cdot\mu$m, the value is multiplied by the channel width.

In this review, the different methods of forming covalent contacts, from the formation of defects by particle irradiation, annealing, formation of edge contacts, to patterning, are reviewed. Additionally, since covalent contacts are crucial for the lowering of the energy barrier by providing orbital hybridization and for reducing the contact resistance at the metal-graphene interface, the resulting contact resistances gathered from the different methods are also reviewed. Finally, this review also provides the limitations of each method of forming covalent contacts.

II. Formation of Defects by Particle Irradiation

In order to create unstable dangling carbon bonds in the graphene lattice for metal-graphene covalent bonding, the carbon atoms are removed by particle irradiation, creating defect sites, or vacancies. When high-energy particles collide with the carbon atoms of graphene, they transfer energy to the target atoms, allowing them to acquire sufficient energy for their extraction from the lattice site [37,38]. Fig. 1(a) shows a graphene lattice with a missing carbon, which has been ejected by proton irradiation. This type of defect site is called an unreconstructed monovacancy [39], in which the dangling bonds do not bond with each other and remain free. Thus, with defects induced in the lattice, these free dangling bonds remain for the covalent bonding to the metals. As a result, covalent contacts can be formed at the defect sites, thereby reducing the contact resistance. The improvement in device performance has been shown by Meersha et al., where a metal-graphene contact resistance of 700 $\Omega\cdot\mu$m is obtained from a CVD-grown graphene device under Ar ion bombardment at an exposure time of 20 s [40].

Another example is the "gentle" low-power O_2 plasma treatment of the device for the creation of defects on the graphene site. O_2 plasma treatment is the exposure of the target to a high-energy O_2 plasma, a process much similar to particle irradiation. Except, in this case, when the O_2 plasma hits, the oxygen molecules bond with the carbon atoms of graphene and form CO_2 molecules as a byproduct, as well as C-O bonds in the graphene sheet in place of C-C bonds. Thus, during metallization, the metals are able to chemically bond with the oxygen atoms and ultimately form C-M bonds. Consequently, covalent contacts are achieved at the metal-graphene interface. Using this mechanism, Robinson et al. found that increasing the O_2 plasma treatment time up to 90 s improved the specific contact resistance due to the creation

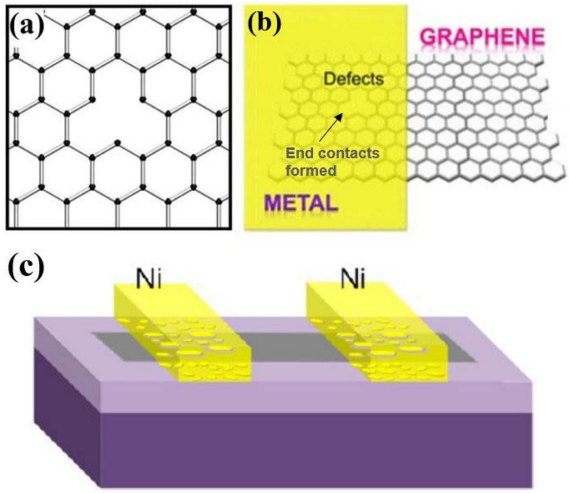

Figure 1. (a) Schematic representation of an unreconstructed monovacancy in the graphene lattice. (b) Vacant sites created in the graphene sheet from the dissolution of carbon atoms into the metal due to annealing. The metal is one that allows for chemisorption at the interface. (c) Ni electrodes deposited on top of the previous structure, which contains etched pits from annealing the previous Ni-graphene device. (Part a reprinted with permission from 38, copyright © 2017 Royal Society of Chemistry. Part b reprinted (adapted) with permission from 44, copyright © 2017 American Chemical Society. Part c reprinted (adapted) with permission from 45, copyright © 2017 American Chemical Society.)

of the defect sites that lead to covalent bonding of the metal to the underlying graphene [41].

However, the downside to these techniques is the introduction of too many defects into the graphene lattice, which can occur if the sheet is exposed to the high-energy source for too long. Because defects are randomly distributed when formed by particle irradiation of the target over large areas, and because they are more likely to be generated in already-existing vacancies due to increased strain in those areas [42], there is a risk of over-generating defects in the lattice. Defects impede carrier transfer because they scatter electrons. Hence, when there are too many vacancies in the graphene site, too much scattering occurs. From the previous example, Meersha et al. also showed that with an increase in Ar ion irradiation time, an upturn in the contact resistance graph was shown, where the contact resistance first decreased and then increased; and Robinson et al. discovered that an exposure time of over 90 s resulted in a higher specific contact resistance. Ultimately, the contact resistance increases when defects dominate. Because particle irradiation leads to an upturn in the contact resistance beyond the optimal exposure time due to the eventual creation of too many defects into the graphene lattice, it is not an efficient approach to lowering the contact resistance of the device.

III. Formation of Covalent Contacts by Annealing

Annealing previously has been known to improve metal-graphene adhesion by removing surface contaminants at the interface. For instance, Lin et al. discovered that annealing the graphene surface at 200 °C for 2 h decomposed the PMMA residues that remained from imperfect PMMA etching [43]. However, it has been discovered thereafter that annealing the graphene while it is in contact with the metal results in the formation of covalent contacts by dissolving the carbon atoms in the graphene lattice. The carbon atoms can be dissolved when in contact with certain metals, like Ni, Pd, and Ti, due to chemisorption at the interface, where the metal's *d*-orbitals and graphene's π-orbitals become hybridized, resulting in a strong interaction [44]. Thus, when the graphene is annealed while in contact with the metals that allow for chemisorption, the chemical reaction of the graphene and the Ni is enhanced, so carbon atoms dissolve into the metal, leaving behind vacancies. Fig. 1(b) shows the formation of unreconstructed monovacancies from annealing the device. During metallization, covalent contacts are formed at the vacant sites, whereas top contacts are formed in the remaining areas. The phenomenon of carbon dissolution due to annealing was explained by Leong et al. in their study on the effect of annealing on metal-graphene interfaces [45]. Annealing their Ni-contacted graphene device at 300 °C for 1 h showed a much higher D-band Raman intensity than just annealed graphene and Ni-contacted graphene without anneal, which correlates to the carbon dissolution.

Additionally, Leong et al. in a prior experiment described the annealing phenomenon in terms of metal etching of the graphene [46]. As a result of annealing their Ni-contacted graphene device at 580 °C for 0.5 h, pits in the graphene sheet were etched by the Ni that became isolated into small particles. By etching the graphene, the dangling bonds became exposed at the etched sites; so, the pits became areas of covalent contacts. Fig. 1(c) shows the device schematic, where the Ni electrodes are deposited on top of the annealed structure. The newly-deposited Ni is in covalent contact with graphene in the etched areas and top contact in the others. As expected, annealing showed an improvement in the device performance, with a contact resistance of 89 Ω·μm with treatment compared to that of 294 Ω·μm without treatment.

However, both experiments by Leong et al. showed that extending the annealing time does not further reduce the contact resistance significantly. This is simply due to the nature of graphene, as defects in the sheet, as well as the area of graphene, limit the amount of dangling bonds that can be formed.

IV. Formation of Edge Contacts by O_2 Plasma Treatment

So far, the formation of covalent contacts by high-energy and high-temperature means has shown to reduce the contact resistance of the graphene device, but only up to the optimal exposure time or temperature. Because finding the optimal condition in each case for device fabrication is troublesome, researchers have looked for new ways to achieve covalent contacts. Of those researchers, Wang et al. has discovered a new contact geometry, where the metals bind to the graphene just at its edge [20]. This type of contact geometry leads to a type of metal-graphene covalent contact called one-dimensional or edge contacts, where the metals are bonded to the graphene just at the

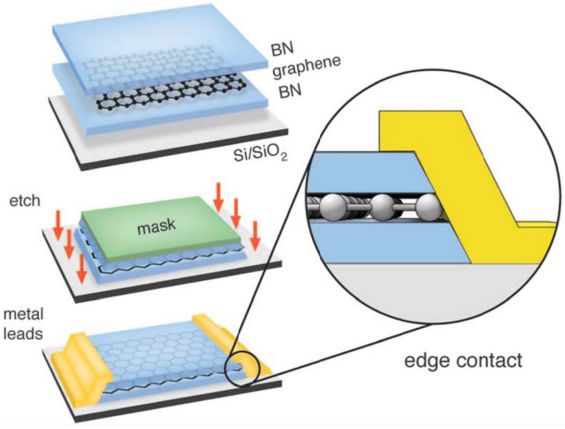

Figure 2. Edge contact of the metal to the BN/graphene/BN heterostructure. The three-dimensional metal is in contact with the two-dimensional graphene just at its edge. (Reprinted with permission from 20, copyright © 2017 The American Association for the Advancement of Science.)

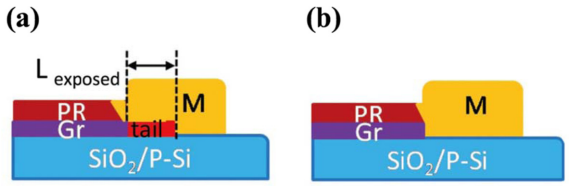

Figure 3. O_2 plasma treatment of graphene to etch the material for the creation of edge contacts. Treatment times are (a) 5-10 s to 35 s, where the shortening of the exposed graphene contact length ($L_{exposed}$) is seen; and (b) 35 s to 45 s, where the exposed graphene is completely etched. (Parts a and b reprinted with permission from 46, copyright © 2017 Royal Society of Chemistry.)

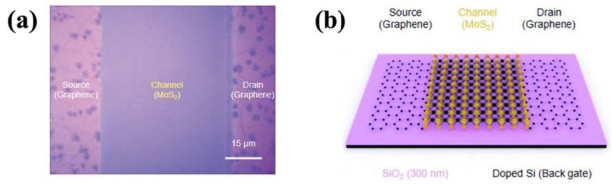

Figure 4. Graphene-MoS_2 heterojunction-based, back-gate FET device shown (a) under an optical microscopy and (b) as a schematic illustration, both showing edge contacts of MoS_2 channel layer to the graphene electrodes. (Parts a and b reprinted with permission from 47, copyright © 2017 Royal Society of Chemistry.)

edge of the graphene sheet. In order to achieve these contacts, the graphene sheet is first encapsulated in boron nitride in a BN/graphene/BN heterostructure before the plasma-etching of the edges at opposing sides; then, the metal is deposited just at the exposed edges by electron beam evaporation for the successful formation of metal-graphene edge contacts. Fig. 2 shows the device structure, where the metal electrodes are in contact with the heterostructure just at its edge. The resulting performance of this device is exceptional, with a room-temperature mobility of 140,000 cm^2/Vs and a contact resistance of about 150 Ω·μm at large carrier densities, which, at its time, was about 25% lower than the value achieved by the device in traditional top-contact configuration [20].

However, because of the complexity of the heterostructure, the efficiency of this device fabrication is not great. Conversely, Yue et al. has discovered a method utilizing O_2 plasma treatment to create edge contacts without the need for the complex heterostructure [28]. By etching graphene in the areas for the metals to be deposited, edge contacts can be achieved. Fig. 3 shows the schematic of etching the graphene via O_2 plasma treatment for the creation of edge contacts. In Fig. 3(a), when graphene is exposed to the treatment for over 5-10 s and under 35 s, the area of the graphene that is not protected by the photoresist becomes etched, and the exposed length, $L_{exposed}$, becomes shorter; hence, if the metal were deposited, a complete edge contact would not be achieved, as there would be graphene remaining under the deposited metal. In Fig. 3(b), however, edge contacts are achieved when graphene is exposed to the treatment for over 35 s and under 45 s, since the graphene in the area for metal to be deposited is completely etched. Thus, when the metal is deposited, it covalently bonds to the graphene at its edge, resulting in orbital hybridization at the interface. Additionally, due to the faster carrier transfer from the shorter bonding distance achieved by edge contacts, the device showed its best contact resistance of 270 Ω·μm at room temperature when exposed for 45 s. Yet, since the O_2 plasma treatment creates defects, as do particle irradiation, optimal exposure time must again be considered for the best device performance yield. In the aforementioned study, an exposure time over 45 s has led to over-etching of graphene, in which metal-graphene contact was decreased, and an exposure time under 5 s has led to under-etching, in which not enough covalent contacts were formed for a significant decrease in the contact resistance.

Chen et al. has expanded on this O_2 plasma mechanism of creating edge contacts by etching the graphene sheet and directly growing MoS_2 via CVD for the fabrication of a device geometry in which graphene acted as the electrodes [47]. Thus, by this mechanism, the interface contains graphene and another two-dimensional material rather than a three-dimensional metal. Previously, it has shown that CVD growth of MoS_2 is possible on SiO_2 substrate [48,49], yet this method has not been used before for the implementation of MoS_2 in edge-contact geometry to graphene. To fabricate this graphene-MoS_2 heterojunction-based FET device, O_2 plasma treatment is used to etch away the graphene sheet only at the center before CVD-growth of MoS_2. As a result, the MoS_2 layer grows at the exposed center on the SiO_2 and forms the channel, and the graphene at the opposite ends becomes the electrodes, as shown via optical image in Fig. 4(a) and via schematic illustration in Fig. 4(b). Although this device showed typical electrical performances of *n*-type devices, the field-effect mobility of only about 0.46 cm^2/Vs was obtained due to the small grain size of MoS_2. Even with poor device performance, this approach still has the potential for improvement since O_2 plasma treatment was used for the fabrication of a more advanced device geometry that utilizes electrode-channel edge contacts.

V. Patterning the Graphene at the Device Interface

Covalent contacts can also exist under the area of metal-graphene contact, rather than only at the edges of graphene. This contact geometry is achieved by directly patterning the graphene sheet in the areas where the metal will later be deposited. Patterning is done by exposing certain areas of graphene to O_2 plasma in order to etch graphene in a specific pattern for the reduction of contact resistance via covalent contacts. Although various device patterns are possible for fabrication, this review will focus on the holes, comb, rail, and snake patterns. Song et al. etched holes, or antidot arrays, of varying radii in the graphene sheet under the metal-graphene contact area using O_2 plasma treatment

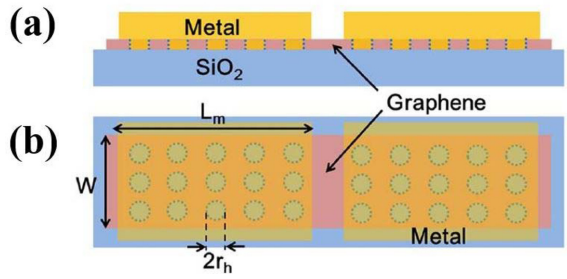

Fig. 5. (a) Device schematic, in which the holes are etched only in the areas of metal contact. Covalent contacts are achieved at the perimeter of the holes, and top contacts exist in the remaining areas. (b) Schematic of the hole pattern of the graphene device, in which the holes are arranged evenly under the contact area. L_m is the length of the metal, W is the width of graphene, and r_h is the hole radius. (Parts a and b reprinted with permission from 50, copyright © 2017 AIP Publishing LLC.)

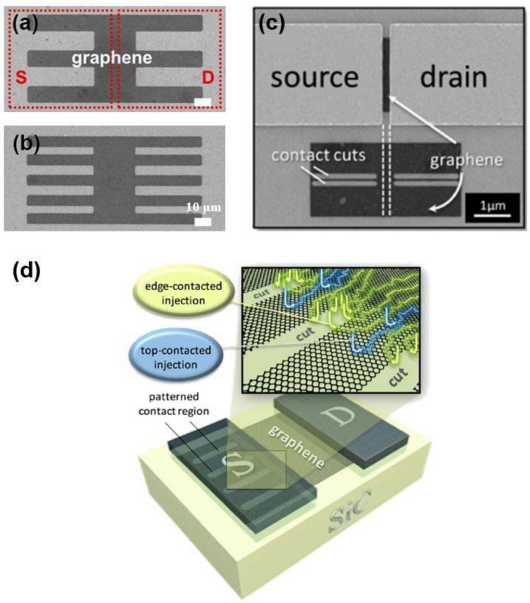

Fig. 6. Comb pattern of the graphene device, in which the peripheral lengths are (a) 312 and (b) 472 μm, respectively. The patterns are made under the metal contact areas, where covalent contacts occur at the edges of the cuts. (c) and (d) Rail pattern of the graphene device, in which the cuts, shown as light gray in the inset, are made under the source and drain areas. Covalent contacts are achieved via dangling bonds at the perimeter of the cuts, whereas top contacts exist in the areas that have not been etched. (Parts a and b reprinted with permission from 52, copyright © 2017 AIP Publishing LLC; and parts c and d reprinted with permission from 53, copyright © 2017 American Chemical Society.)

[50]. Fig. 5(a) shows the schematic of the device, where graphene lies under the metals, except in the areas of the holes, which are etched. At the etched sites, the metal is able to covalently bond with the graphene via the dangling σ-bonds that exist at the perimeter of the holes, shown as the blue dots; at the areas outside of the holes, however, the metal binds to the graphene via van der Waals forces. Hence, both top contacts and covalent contacts exist simultaneously for patterned devices. The holes are more accurately shown in Fig. 5(b), where they are evenly-distributed at the interface of the device. Again, by etching the graphene in certain patterns, the metal is able to bind more strongly to the underlying graphene, thereby lowering the energy barrier at the patterned areas and resulting in a more efficient carrier transfer. In the study, a contact resistance of around 250 Ω·μm was obtained for the devices with holes of 0.38 μm radius, compared to around 650 Ω·μm for the devices without holes. Further, Passi et al. also etched holes in their devices using O_2 plasma treatment [51]. With a stronger metal adhesion to the graphene sheet from covalent contacts at the areas of the holes, a contact resistance of 456 Ω·μm was obtained for the device with holes of 500 nm when distributed evenly under the entire contact area, an improvement from 1518 Ω·μm for the devices without holes. However, this device pattern does not provide enough areas for covalent contacts for a more significant reduction of the contact resistance. So, other device patterns that allow for more covalent contacts should be utilized.

More efficient cuts can be made using the comb pattern, shown in Fig. 6(a) and (b), where parts of the graphene sheet, shown in dark gray, is cut in one end using a similar O_2 plasma etching process. Cho et al. fabricated this pattern to study the dependence of device performance on the peripheral length of graphene [52]. The peripheral length of graphene was increased by increasing the number of cuts, which yielded more dangling bonds bonds at the perimeter of graphene for the formation of covalent contacts at the interface. As the peripheral length increased from 312 mm to 792 μm, a 60% decrease in the contact resistance was shown, and a value of 0.8 kΩ·μm was obtained. This result proves that inducing more cuts improves the strength of the metal-graphene contact for a more efficient device performance.

A pattern similar to the comb geometry is the rail pattern, in which horizontal cuts, shown as light gray, are made in the middle of the graphene sheet, shown as dark gray, at the metal contact area as shown in Fig. 6(c). Hence, dangling bonds exist at the perimeter of the cuts, where the metal can bind covalently. It is notable that the cuts are not extended to the end of graphene, which would result in a comb pattern. Smith et al. fabricated the rail-patterned graphene device using different number of cuts to increase the perimeter length of graphene for their study on the device performance based on the amount of cuts made [53]. Their TLM measurements yielded a contact resistance of 125 Ω·μm post-anneal with 10 cuts under Cu contact, compared to 184 Ω·μm post-anneal without any patterns, which proves that the patterns provide a better device performance via covalent contacts. This proof is shown as the device schematic in Fig. 6(d), where covalent contacts only exist at the edge of the cut areas, providing a fast carrier injection from the metal to the underlying graphene due to a shorter bonding distance. Furthermore, their study showed that as the perimeter length increased, more areas

Table 1. Summary of the contact resistances obtained before and after using various methods per strategies for graphene-based transistors

Strategy	Method	Contact resistance before (O-nm)	Contact resistance after (Ω·μm)	Reference
Defects	AT bombardment	3050	700	40
Annealing	Etched pits	294	89	46
Edge contacts	BN/graphenc/BN heterostrucoire	*	150	20
Patterning	O2 plasma treatment	4762	207	28
	Holes	1518	456	51
	Comb	*	800	52
	Rail	184	125	53
	Snake	1400	484	54

***The contact resistance values for the devices before the treatments were not studied.**

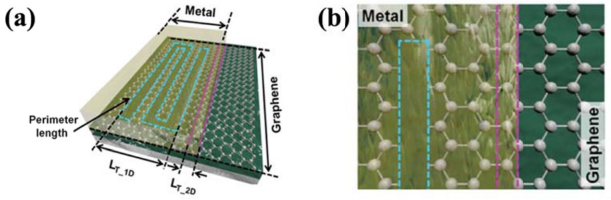

Figure 7. (a) Snake pattern of the graphene device, where L_{T_1D} is the effective transfer length of the etched area, and L_{T_2D} is the effective transfer length of the surface area. (b) Dangling bonds exist at the edges of the etched area of the graphene lattice, shown in cyan, whereas no dangling bonds exist at the surface of the graphene, shown in pink. (Parts a and b reprinted with permission from 54, copyright © 2017 John Wiley and Sons.)

of graphene become available for covalent contacts, and a decrease in the total resistance of the device post-anneal was first seen. Yet, as the number of cuts increased beyond 8, an upturn of the resistance was shown because extreme narrowing of the width of the graphene nanoribbons by making too many cuts had led to quantization effects that impeded carrier transfer at the interface [53]. Because this pattern works best under optimal conditions, in which the perimeter length is kept as large as possible while maintaining a large enough graphene nanoribbon width, a significant limitation exists for this device pattern.

Another type of pattern geometry is the snake pattern, where horizontal cuts are made to connect the long vertical cuts in a snake-like fashion as shown in Fig. 7(a). Park et al. fabricated this pattern on the graphene sheet at the interface of the device, and when the width of the gap between the cut graphene nanoribbons was decreased to 1 μm, a contact resistance of 484 Ω·μm under Pd contact was obtained [54], compared to 1.4 Ω·μm without patterning. Again, the reduction in the contact resistance is due to the dangling bonds that exist at the etched areas, as shown in Fig. 7(b), resulting in covalent contacts at the interface.

VI. Conclusions

This review has discussed the different methods of forming covalent contacts for the reduction of the contact resistance, essentially to realize high-performance graphene transistors. Defects in the graphene sheet created by particle irradiation provide dangling bonds for metal-graphene covalent bonding at the interface of the defect sites. Additionally, annealing enhances the chemical reaction at the chemisorption interfaces and results in the dissolution of the carbon atoms to the metal, as well as a strong orbital hybridization.

This review has also discussed the reduction of the contact resistance by altering the contact geometry of the device. By depositing the metal just at the edge of the graphene layer, edge contacts are achieved that provides covalent bonding of the metal to the graphene. Furthermore, patterning the graphene at the interface strengthens the metal adhesion through covalent contacts provided by the etched areas.

The contact resistance values obtained by the various methods of forming covalent contacts are summarized in Table 1. It is conclusive that covalent contacts are fundamental for the reduction in the contact resistance and the realization of high-performance graphene-based transistors.

Acknowledgements

This research was supported by the MSIT (Ministry of Science and ICT), Korea, under the ICT Consilience Creative program (IITP-2017-2017-0-01015) supervised by the IITP (Institute for Information & communications Technology Promotion) and also under the “Mid-career Researcher Program” (NRF-2016R1A2B2014612) supervised by the NRF (National Research Foundation).

References

[1] F. Bonaccorso, Z. Sun, T. Hasan, and A. C. Ferrari, Nat. Photon. 4, 611 (2010).
[2] R. R. Nair, P. Blake, A. N. Grigorenko, K. S. Novoselov, T. J. Booth, T. Stauber, N. M. Peres, and A. K. Geim, Science. 320, 1308 (2008).
[3] D. Prezzi, D. Varsano, A. Ruini, A. Marini, and E. Molinari, Phys.

Rev. B. 77, 041404 (2008).
[4] A. C. Neto, F. Guinea, N. M. Peres, K. S. Novoselov, and A. K. Geim, Rev. Mod. Phys. 81, 109 (2009).
[5] K. S. Novoselov, S. V. Morozov, T. M. Mohinddin, L. A. Ponomarenko, D. C. Elias, R. Yang, I. I. Barbolina, P. Blake, T. J. Booth, D. Jiang, J. Giesbers, E. W. Hill, and A. K. Geim, Phys. Status Solidi B. 244, 4106 (2007).
[6] K. S. Novoselov, A. K. Geim, S. V. Morozov, D. Jiang, M. I. Katsnelson, I. V. Grigorieva, S. V. Dubonos, and A. A. Firsov, Nature. 438, 197 (2005).
[7] C. Lee, X. Wei, J. W. Kysar, and J. Hone, Science. 321, 385 (2008).
[8] F. Ding, H. Ji, Y. Chen, A. Herklotz, K. Dörr, Y. Mei, A. Rastelli, and O. G. Schmidt, Nano Lett. 10, 3453 (2010).
[9] S. Ghosh, I. Calizo, D. Teweldebrhan, E. P. Pokatilov, D. L. Nika, A. A. Balandin, W. Bao, F. Miao, and C. N. Lau, Appl. Phys. Lett. 92, 151911 (2008).
[10] A. A. Balandin, S. Ghosh, W. Bao, I. Calizo, D. Teweldebrhan, F. Miao, and C. N. Lau, Nano Lett. 8, 902 (2008).
[11] K. S. Kim, Y. Zhao, H. Jang, S. Y. Lee, J. M. Kim, K. S. Kim, J. H. Ahn, P. Kim, J. Y. Choi, and B. H. Hong, Nature. 457, 706 (2009).
[12] S. Bae, H. Kim, Y. Lee, X. Xu, J. S. Park, Y. Zheng, J. Balakrishnan, T. Lei, H. R. Kim, Y. I. Song, Y. J. Kim, K. S. Kim, B. Özyilmaz, J. H. Ahn, B. H. Hong, and S. Iijima, Nat. Nanotechnol. 5, 574 (2010).
[13] J. Han, J. Y. Lee, and J. S. Yeo, Carbon. 105, 205 (2016).
[14] Y. Wang, X. Chen, Y. Zhong, F. Zhu, and K. P. Loh, Appl. Phys. Lett. 95, 209 (2009).
[15] J. Shen, Y. Zhu, X. Yang, and C. Li, Chem. Commun. 48, 3686 (2012).
[16] Y. Shao, J. Wang, H. Wu, J. Liu, I. A. Aksay, and Y. Lin, Electroanalysis. 22, 1027 (2010).
[17] F. Schwierz, Nat. Nanotechnol. 5, 487 (2010).
[18] I. Meric, M. Y. Han, A. F. Young, B. Ozyilmaz, P. Kim, and K. L. Shepard, Nat. Nanotechnol. 3, 654 (2008).
[19] F. Xia, D. B. Farmer, Y.-m. Lin, and P. Avouris, Nano Lett. 10, 715 (2010).
[20] L. Wang, I. Meric, P. Y. Huang, Q. Gao, Y. Gao, H. Tran, T. Taniguchi, K. Watanabe, L. M. Campos, D. A. Muller, J. Guo, P. Kim, J. Hone, K. L. Shepard, and C. R. Dean, Science. 342, 614 (2013).
[21] L. D. Carr, and M. T. Lusk, Nature Nanotechnol. 5, 316 (2010).
[22] Q. Zheng, Y. Geng, S. Wang, Z. Li, and J. K. Kim, Carbon. 48, 4315 (2010).
[23] C. Wang, Y. Liu, L. Lan, and H. Tan, Nanoscale. 5, 4454 (2013).
[24] P. Sutter, J. T. Sadowski, and E. Sutter, Phys. Rev. B. 80, 245411 (2009).
[25] S. Y. Zhou, G. H. Gweon, A. Fedorov, P. First, W. De Heer, D. H. Lee, F. Guinea, A. C. Neto, and A. Lanzara, Nat. Mater. 6, 770 (2007).
[26] M. Ishigami, J. H. Chen, W. G. Cullen, M. S. Fuhrer, and E. D. Williams, Nano Lett. 7, 1643 (2007).
[27] A. Pirkle, J. Chan, A. Venugopal, D. Hinojos, C. W. Magnuson, S. McDonnell, L. Colombo, E. M. Vogel, R. S. Ruoff, and R. M. Wallace, Appl. Phys. Lett. 99, 122108 (2011).
[28] D. W. Yue, C. H. Ra, X. C. Liu, D. Y. Lee, and W. J. Yoo, Nanoscale. 7, 825 (2014).
[29] G. Giovannetti, P. Khomyakov, G. Brocks, V. M. Karpan, J. van den Brink, and P. J. Kelly, Phys. Rev. Lett. 101, 026803 (2008).
[30] K. Nagashio and A. Toriumi, Jpn. J. Appl. Phys. 50, 070108 (2011).
[31] C. W. Chen, F. Ren, G. C. Chi, S. C. Hung, Y. P. Huang, J. Kim, I. I. Kravchenko, and S. J. Pearton, J. Vac. Sci. Technol., B. 30, 060604 (2012).
[32] W. Li, Y. Liang, D. Yu, L. Peng, K. P. Pernstich, T. Shen, A. R. Hight Walker, G. Cheng, C. A. Hacker, C. A. Richter, Q. Li, D. J. Gundlach, and X. Liang, Appl. Phys. Lett. 102, 183110 (2013).
[33] S. K. Hong, S. M. Song, O. Sul, and B. J. Cho, Carbon Lett. 14, 171 (2013).
[34] A. D. Franklin, S. J. Han, A. A. Bol, and V. Perebeinos, IEEE Electron Device Lett. 33, 17 (2012).
[35] A. Hsu, H. Wang, K. K. Kim, J. Kong, and T. Palacios, IEEE Electron Device Lett. 32, 1008 (2011).
[36] Q. Gao and J. Guo, APL Mater. 2, 056105 (2014).
[37] A. Krasheninnikov and F. Banhart, Nat. Mater. 6, 723 (2007).
[38] J. Han, J. Y. Lee, J. Choe, and J. S. Yeo, RSC Adv. 6, 76273 (2016).
[39] O. Lehtinen, I. L. Tsai, R. Jalil, R. R. Nair, J. Keinonen, U. Kaiser, and I. V. Grigorieva, Nanoscale. 6, 6569 (2014).
[40] A. Meersha, H. B. Variar, K. Bhardwaj, A. Mishra, S. Raghavan, N. Bhat, and M. Shrivastava, IEEE IEDM, 5.3.1 (2016).
[41] J. A. Robinson, M. LaBella, M. Zhu, M. Hollander, R. Kasarda, Z. Hughes, K. Trumbull, R. Cavalero, and D. Snyder, Appl. Phys. Lett. 98, 053103 (2011).
[42] F. Banhart, J. Kotakoski, and A. V. Krasheninnikov, ACS Nano. 5, 26 (2010).
[43] Y. C. Lin, C. C. Lu, C. H. Yeh, C. Jin, K. Suenaga, and P. W. Chiu, Nano Lett. 12, 414 (2011).
[44] C. Gong, G. Lee, B. Shan, E. M. Vogel, R. M. Wallace, and K. Cho, J. Appl. Phys. 108, 123711 (2010).
[45] W. S. Leong, C. T. Nai, and J. T. Thong, Nano Lett. 14, 3840 (2014).
[46] W. S. Leong, H. Gong, and J. T. Thong, ACS Nano. 8, 994 (2013).
[47] X. Chen, Y. J. Park, T. Das, H. Jang, J. B. Lee, and J. H. Ahn, Nanoscale. 8, 15181 (2016).
[48] Y. H. Lee, X. Q. Zhang, W. Zhang, M. T. Chang, C. T. Lin, K. D. Chang, Y. C. Yu, J. T. W. Wang, C. S. Chang, L. J. Li, and T. W. Lin, Adv. Mater. 24, 2320 (2012).
[49] Y. Yu, C. Li, Y. Liu, L. Su, Y. Zhang, and L. Cao, Sci. Rep. 3, 1866 (2013).
[50] S. M. Song, T. Y. Kim, O. J. Sul, W. C. Shin, and B. J. Cho, Appl. Phys. Lett. 104, 183506 (2014).
[51] V. Passi, A. Gahoi, J. Ruhkopf, S. Kataria, F. Vaurette, E. Pallecchi, H. Happy, and M. C. Lemme, IEEE, 236 (2016).
[52] C. Cho, S. K. Lee, J. W. Noh, W. Park, S. Lee, Y. G. Lee, H. J. Hwang, C. G. Kang, M. H. Ham, and B. H. Lee, Appl. Phys. Lett. 106, 213107 (2015).
[53] J. T. Smith, A. D. Franklin, D. B. Farmer, and C. D. Dimitrakopoulos, ACS Nano. 7, 3661 (2013).
[54] H. Y. Park, W. S. Jung, D. H. Kang, J. Jeon, G. Yoo, Y. Park, J. Lee, Y. H. Jang, J. Lee, S. Park, H. Y. Yu, B. Shin, S. Lee, and J. H. Park, Adv. Mater. 28, 864 (2015).